ELSEVIER

Contents lists available at ScienceDirect

# Journal of Computational Physics

www.elsevier.com/locate/jcp



# Data-driven compressive sensing and applications in uncertainty quantification



Hong Liang a,b,1, Qi Sun b,c,\*,1, Qiang Du d

- <sup>a</sup> Zhou-Pei Yuan Center for Applied Mathematics, Tsinghua University, Beijing, 100084, China
- <sup>b</sup> Division of Applied and Computational Mathematics, Beijing Computational Science Research Center, Beijing, 100094, China
- <sup>c</sup> School of Mathematical Science, University of Science and Technology of China, Hefei, 230026, China
- <sup>d</sup> Department of Applied Physics and Applied Mathematics, and Data Science Institute, Columbia University, New York, NY 10027, USA

#### ARTICLE INFO

#### Article history: Received 14 November 2017 Received in revised form 11 May 2018 Accepted 31 July 2018 Available online 3 August 2018

Keywords:
Compressive sensing
Data-driven method
Uncertainty quantification

#### ABSTRACT

In this paper, we propose a data-driven compressive sensing method for the effective and sparse representation of solutions to a stochastic system, in which a problem-dependent basis is constructed and used to exploit the sparse patterns. Given what appears to be a highly incomplete set of sample observations, the essential ingredients of the proposed method involve (i) estimating the covariance function from low-fidelity simulations, (ii) extracting the most dominant energetic modes from the Karhunen-Loève analysis, and (iii) solving the basis pursuit problem associated with data-driven functions for high-fidelity models. Compared with other conventional compressive sensing methods that use a problem-independent basis, our approach can significantly increase the sparsity of expansion coefficients in many situations. When applied to uncertainty quantification problems such as partial differential equations with random input data, numerical experiments are carried out to show the effectiveness of our data-driven method in recovering the sparse solution globally over the physical domain.

© 2018 Elsevier Inc. All rights reserved.

# 1. Introduction

There are many application problems modeled by partial differential equations (PDEs) with random inputs, and the numerical simulation of such systems is often found to be computationally intractable due to the so called "curse of dimensionality" [1,2]. With limited computation and storage capabilities in practice, one of the essential challenges in these applications is to accurately recover the solution when only a limited number of sample observations are provided. Recently, efforts have been made to alleviate this difficulty by exploring the sparse structure of solution at stochastic level, *i.e.*, the evaluation of solution at a single spatial point can be resolved exactly using a few polynomial chaos (PC) basis [3–5]. However, to recover such a solution globally over the physical domain, typical compressive sensing (CS) methods may require many thousands of degrees of freedom, and where they are available are not affordable to most feedback control problems due to the demand on the controller design in real time with limited computing resources [6–8]. By constructing basis functions that are intimately connected to the problem being studied, the data-driven compressive sensing (DCS) method

<sup>\*</sup> Corresponding author at: Division of Applied and Computational Mathematics, Beijing Computational Science Research Center, Beijing, 100094, China. E-mail addresses: liang-h13@mails.tsinghua.edu.cn (H. Liang), sunqi@csrc.ac.cn (Q. Sun), qd2125@columbia.edu (Q. Du).

<sup>&</sup>lt;sup>1</sup> The first two authors made equal contributions to this manuscript.

proposed here offers an effective approach for model reduction without resorting to additional assumptions, which can be highly desirable in practice.

Specifically, we consider the solution to a stochastic system that is represented in terms of deterministic and stochastic basis functions [3,1,9,10,2]. Let  $(\Omega, \mathcal{F}, \mathcal{P})$  be a complete probability space, and let D be a bounded Lipschitz domain in  $\mathbb{R}^r$  where  $r \in \mathbb{Z}_+$ . We also denote by  $\mathcal{T}_h$  a conforming tessellation of D with maximum mesh size h > 0. In the context of stochastic finite element methods [1], a fully discrete approximation of the solution  $u(x, \xi) : D \times \Omega \to \mathbb{R}$  takes on the form (not relabeled)

$$u(x,\xi) = \sum_{i=1}^{p} \sum_{j=1}^{m} c_{ij} \varphi_j(x) \psi_i(\xi),$$
 (1)

where  $c_{ij} \in \mathbb{R}$  are coefficients with respect to (w.r.t.) a set of finite element basis  $\{\varphi_j(x)\}_{j=1}^m$ , e.g., piecewise linear functions that are adopted to effect discretization w.r.t.  $x \in D$ , and  $\{\psi_i(\xi)\}_{i=1}^p$  represents a set of multivariate PC basis, e.g., Legendre polynomials or Hermite polynomials that are orthonormal w.r.t. the joint probability measure  $\rho(\xi)$  of a d-dimensional random variable  $\xi = (\xi_1(\omega), \dots, \xi_d(\omega))$  for almost everywhere  $\omega \in \Omega$ .

To determine the coefficients in expansion (1), the collocation method is utilized in conjunction with appropriate stochastic and deterministic collocation points, i.e.,  $\{\xi_i\}_{i=1}^n$  and  $\{x_j\}_{j=1}^m$  respectively. We then arrive at the linear system

$$\begin{pmatrix} u(x_1, \boldsymbol{\xi}_1) \cdots u(x_m, \boldsymbol{\xi}_1) \\ \vdots & \vdots \\ u(x_1, \boldsymbol{\xi}_n) \cdots u(x_m, \boldsymbol{\xi}_n) \end{pmatrix} = \begin{pmatrix} \psi_1(\boldsymbol{\xi}_1) \cdots \psi_p(\boldsymbol{\xi}_1) \\ \vdots & \vdots \\ \psi_1(\boldsymbol{\xi}_n) \cdots \psi_p(\boldsymbol{\xi}_n) \end{pmatrix} \begin{pmatrix} c_{11} \cdots c_{1m} \\ \vdots & \vdots \\ c_{p_1} \cdots c_{p_m} \end{pmatrix} \begin{pmatrix} \varphi_1(x_1) \cdots \varphi_1(x_m) \\ \vdots & \vdots \\ \varphi_m(x_1) \cdots \varphi_m(x_m) \end{pmatrix}$$

which for simplicity is denoted by

$$\mathbf{u} = \Psi \mathbf{c} \Phi. \tag{2}$$

Here,  $\mathbf{u} := (u(x_i, \boldsymbol{\xi}_j))$  is the matrix of observations,  $\mathbf{c} := (c_{ij})$  is the coefficient matrix to be determined,  $\boldsymbol{\Psi} := (\psi_i(\boldsymbol{\xi}_j))$  and  $\boldsymbol{\Phi} := (\varphi_i(x_j))$  represent the spatial and stochastic information matrices respectively. Typically, the stochastic degree of freedoms p (and consequently the total number of unknowns  $m \times p$ ) grows quickly in the dimension of random input data  $\boldsymbol{\xi}$ . Consequently, with a smaller number of equations than unknowns, *i.e.*, n < p or even  $n \ll p$ , the linear system (2) becomes underdetermined and has infinitely many solutions provided that at least one solution exists.

Thanks to the celebrated works on CS methods [11,3,12], it is possible to recover the unique solution of problem (2) from what appears to be a highly incomplete set of sample observations. In other words, given that the expansion coefficients are sparse w.r.t. their associated basis functions, an accurate approximate solution can be constructed by solving the basis pursuit (BP) problem [13]. In the spirit of such discovery, much attention has been devoted to the recovery of the solution at a single spatial point [14,4]. Generically, different sparse patterns may result at different points. Taking such CS approaches, there may still be a moderate amount of coefficients contributing to the representation of solution over the entire spatial domain, which makes computation expensive for various application problems.

The major contribution of this work is to introduce a problem-dependent basis for the expansion (1), which further enhances sparsity in the representation of solution and hence improves the recovery accuracy. To be specific, we firstly construct the covariance function  $Cov_u(x, x')$  of solution  $u(x, \xi)$  using low-fidelity simulations which are less accurate but computationally cheaper than high-fidelity ones [15]. Then, the widely studied Karhunen-Loève (KL) analysis, based on the integral equation

$$\int_{D} \text{Cov}_{u}(x, x')\phi_{j}(x') dx' = \lambda_{j}\phi_{j}(x), \tag{3}$$

with a sequence of eigenpairs  $(\lambda_j, \phi_j(x))_{j\geqslant 1}$ , is applied to extract the most dominant energetic modes as our data-driven basis functions. In particular, the collection of primary energetic modes remains almost unchanged as the spatial resolution increases. As a result, by using the basis functions generated from low-fidelity models, *e.g.*, coarse mesh solutions, we may have little loss in accuracy for fast recovery of the high-fidelity models such as those based on fine mesh simulations. The representation of solution is now given by

$$u(x,\boldsymbol{\xi}) = \sum_{i=1}^{p} \sum_{j=1}^{m} \tilde{c}_{ij} \phi_j(x) \psi_i(\boldsymbol{\xi}), \tag{4}$$

where the expansion coefficients are determined by solving the BP problem associated with the data-driven basis.

To demonstrate the enhancement of sparsity for the proposed DCS method, we consider first the projection of expansion (1) into the space spanned by eigenfunctions  $\{\phi_j\}_{j=1}^m$  in (3), where the coefficients can be bounded by the eigenvalues. Since these eigenvalues are often found to decay very quickly in many applications [16], such a representation can be used

to compress the coefficients, although it might favor the basis functions with small eigenvalues. Accordingly, to further increase the sparsity, an  $\ell_1$ -norm minimization problem is introduced instead, in which the restricted isometry property (RIP) constant remains the same as the conventional CS methods. Numerical experiments are carried out to validate our theoretical findings.

The paper is organized as follows. In section 2, a brief introduction to the CS and PC methods is illustrated. Next, in section 3, we present an algorithm for the efficient extraction of data-driven basis, as well as a mathematical study of the optimality of such basis functions. Then, the discussion on DCS method is given in section 4. Numerical examples with high compressibility and applications in uncertainty quantification are reported in section 5 to validate the effectiveness of our method. Finally, we end by drawing some conclusions and indicating possible future works in section 6.

### 2. Preliminary

We first briefly recall some basic theory of PC expansion, CS techniques and some notations used in this work,

#### 2.1. Polynomial chaos expansions

Let  $(\Omega, \mathcal{F}, \mathcal{P})$  be a complete probability space defined as before. To start with the PC expansion, we define a set of multi-indices with a finite number of non-negative integers as follows:

$$\mathcal{I}_{p_r}^d := \left\{ \boldsymbol{\alpha} = (\alpha_1, \alpha_2, \cdots \alpha_d) : \alpha_i \in \mathbb{N}_0^+, \ |\boldsymbol{\alpha}| = \sum_{i=1}^d \alpha_i < p_r \right\}.$$

For any function  $u(x, \xi) \in L^2(D) \otimes L^2(\Omega)$ , the associated generalized PC expansion takes the form

$$u(x, \xi) = \sum_{\alpha \in \mathcal{I}_{\infty}^{d}} b_{\alpha}(x) \psi_{\alpha}(\xi)$$
 (5)

where  $b_{\alpha}(x)$  are the coefficients, and  $\psi_{\alpha}(\xi)$  are the multivariate polynomials basis which are constructed by the tensor product of univariate orthonormal polynomials.

Without loss of generality, the univariate random variable  $\xi$  is assumed to satisfy the uniform distribution on  $\Omega = [-1, 1]$ , then we obtain the Legendre polynomials according to the Askey scheme [17] for non-negative integer n, *i.e.*,

$$\ell_n(\xi) = \sqrt{\frac{2n+1}{2}} \frac{1}{2^n n!} \frac{d^n}{d\xi^n} \left[ \left( \xi^2 - 1 \right)^n \right],$$

which form a complete orthonormal basis of  $L^2(\Omega)$  w.r.t. the weighting function  $\rho(\xi) = \frac{1}{2}$ . Clearly, tensor products of the elements  $\{\ell_n(\xi_i)\}_{n=0}^{\infty}$ , where  $i=1,\ldots,d$ , construct a complete basis of the corresponding d-dimensional probability space. That is, for a multi-index  $\alpha \in \mathcal{I}_{\infty}^d$ , the d-dimensional polynomial  $\psi_{\alpha}$  of order  $|\alpha|$  is defined as

$$\psi_{\alpha}(\boldsymbol{\xi}) := \prod_{i=1}^{d} \ell_{\alpha_i}(\xi_i),$$

which is orthonormal w.r.t. the joint probability measure  $\rho(\xi) = \prod_{i=1}^d \rho(\xi_i)$  for  $\xi \in \Omega = [-1, 1]^d$  (not relabeled), i.e.,

$$\int_{\Omega} \psi_{\alpha}(\xi) \psi_{\beta}(\xi) \rho(\xi) d\xi := \mathbb{E} \left[ \psi_{\alpha} \psi_{\beta} \right] = \delta_{\alpha\beta},$$

for any  $\alpha, \beta \in \mathcal{I}_{\infty}^d$ , where  $\delta_{\alpha\beta}$  represents the Kronecker delta function.

Note that the possible infinite summation has been truncated to only p terms for the convenience of our discussion, where  $p = \frac{(p_r + d)!}{p_r \cdot d!}$  is the cardinality of the stochastic polynomial basis. After mapping the multiple indices associated with the PC basis functions to the single index [18], the expansion (5) can be rewritten as

$$u(x, \xi) = \sum_{i=1}^{p} b_i(x) \psi_i(\xi)$$
 (6)

where  $\psi_1(\xi) \equiv 1$ . On the other hand, to fully discretize the expansion (6), the standard finite element method is used for the approximation of coefficients  $b_i(x)$  in (6), which results in the stochastic finite element representation (1).

## 2.2. Sparse recovery using compressive sensing

CS methods are effective at recovering the solution (1) from a set of incomplete random measurements, provided that the expansion coefficients are sparse w.r.t. an over-complete dictionary of solution patterns [11,13].

Specifically, by introducing the vectorization of a matrix  $\mathbf{A} \in \mathbb{R}^{m,n}$  as

$$\text{vec}(\mathbf{A}) = (a_{11}, \dots, a_{m1}, \dots, a_{1n}, \dots, a_{mn})^T,$$

and the Kronecker product of the matrix  $\mathbf{A} \in \mathbb{R}^{m,n}$  with another matrix  $\mathbf{B} \in \mathbb{R}^{p,q}$  as

$$\mathbf{A} \otimes \mathbf{B} = \begin{pmatrix} a_{11}\mathbf{B} & \cdots & a_{1n}\mathbf{B} \\ \vdots & \ddots & \vdots \\ a_{m1}\mathbf{B} & \cdots & a_{mn}\mathbf{B} \end{pmatrix}_{mp \times nq},$$

the under-determined linear system (2) can now be rewritten in the vector form

$$\operatorname{vec}(\mathbf{u}) = (\mathbf{\Phi}^T \otimes \mathbf{\Psi}) \operatorname{vec}(\mathbf{c}), \tag{7}$$

where  $\Theta = \Phi^T \otimes \Psi$  serves as a dictionary matrix, the same as the standard CS setting.

Recall that one fundamental premise of CS approach is that the coefficient vector  $\text{vec}(\mathbf{c})$  is sparse w.r.t. the dictionary matrix  $\boldsymbol{\Theta}$ . Typically, the spatial grid points are chosen to be the collocation points  $\{x_i\}_{i=1}^m$  and the spatial information matrix then reduces to an  $m \times m$  identity matrix. As such, a low-rank approximation of solution  $u(x, \boldsymbol{\xi})$  can be constructed by solving the BP problem associated with the constraint equation (7), *i.e.*,

$$\operatorname{vec}(\hat{\mathbf{c}}) = \underset{\operatorname{vec}(\mathbf{c})}{\operatorname{arg\,min}} \| \operatorname{vec}(\mathbf{c}) \|_{1} \text{ subject to } \operatorname{vec}(\mathbf{u}) = \mathbf{\Theta} \operatorname{vec}(\mathbf{c}),$$
(8)

where the dictionary matrix  $\Theta = I_m \otimes \Psi$  contains no prior knowledge of the sparse patterns of solution. In particular, by Lemma 1, the RIP constant for matrix  $\Theta$  in (8) satisfies  $\delta_s(\Theta) = \delta_s(\Psi)$ .

**Lemma 1** ([19,20]). Let **A** be the  $m \times n$  information matrix, the RIP constant of **A** is defined as the smallest number  $\delta_s(\mathbf{A}) \in (0,1)$  such that

$$(1 - \delta_{s}(\mathbf{A})) \|x\|_{2}^{2} \le \|\mathbf{A}x\|_{2}^{2} \le (1 + \delta_{s}(\mathbf{A})) \|x\|_{2}^{2}$$

$$(9)$$

holds for all vectors  $x \in \mathbb{R}^n$  which have at most  $s \in \{1, ..., n\}$  nonzero entries. Similarly, let  $\delta_s(\mathbf{B})$  be the RIP constant for matrix  $\mathbf{B} \in \mathbb{R}^{p,q}$ , then the following estimation holds true:

$$\max\{\delta_{S}(\boldsymbol{A}), \delta_{S}(\boldsymbol{B})\} \leq \delta_{S}(\boldsymbol{A} \otimes \boldsymbol{B}) \leq (1 + \delta_{S}(\boldsymbol{A}))(1 + \delta_{S}(\boldsymbol{B})) - 1 \tag{10}$$

**Lemma 2** ([19,21]). Assume that  $\delta_{2s}(\Theta) \leq \sqrt{2} - 1$ , the solution to (8) satisfies the following error estimate:

$$\|\operatorname{vec}(\mathbf{c}) - \operatorname{vec}(\hat{\mathbf{c}})\|_{2} \le C \frac{\|\operatorname{vec}(\mathbf{c}) - \operatorname{vec}(\mathbf{c}_{s})\|_{1}}{\sqrt{s}}$$
(11)

where the constant C depends only on the RIP constant, and  $vec(\mathbf{c}_s)$  is the s-term approximation of  $vec(\mathbf{c})$  obtained by retaining the s most significant modes.

One can, without question, decouple (8) into m independent subsystems to recover pointwise the global solution, provided that the information matrix  $\Psi$  satisfies certain requirements on the RIP constant [3,4]. However, different spatial points may have different sparse patterns. As a result, there may still be a moderate amount of coefficients contributing to the expansion (1). To further enhance the sparsity as well as the efficiency of the recovery procedure, we propose the concept of "data-driven" compressive sensing to construct a basis which extracts dominant features of the solution from a given "incomplete" set of sample observations in what follows.

#### 3. Data-driven basis selection

Given a limited number of sample simulations, we begin the construction of data-driven basis by first introducing a sparse covariance recovery procedure. Then the widely studied KL analysis (3) is applied to extract energetic solution patterns as our data-driven basis functions, which are shown to be optimal in  $L^2(\Omega) \otimes L^2(D)$  at effectively capturing the essential information in the dataset and enhancing the sparsity.

## 3.1. Sparse recovery of covariance function

As is well known, covariance function characterizes the correlation of a solution  $u(x, \xi)$  with itself at pairs of spatial points and provides sufficient statistics for the KL analysis [21]. However, due to the limited computation and storage resources in practice, an important issue is the recovery of covariance function

$$Cov_{u}(x, x') = \int_{\Omega} u(x, \xi)u(x', \xi)\rho(\xi) d\xi - E_{u}(x)E_{u}(x')$$
(12)

when only a few observations are provided. Here,  $E_u(x)$  denotes the expectation of  $u(x, \xi)$ . Since the Monte Carlo (MC) method typically requires the use of a sufficiently large number of sample simulations to ensure satisfactory accuracy, it may be computationally too demanding to correctly recover the statistical moments in such a situation. Alternatively, given that a solution  $u(x,\xi)$  is sparse w.r.t. the basis functions in (1), the solution and hence its covariance can be accurately recovered using  $n \ll p$  sample measurements via the CS method [3,12]. The details are presented as follows.

### Algorithm 1 Sparse recovery of covariance function.

**Input**: stochastic and spatial collocation points, namely,  $\{\xi_i\}_{i=1}^n$  and  $\{x_i\}_{i=1}^m$ .

**Output**: covariance function  $Cov_{\hat{u}}(x, x')$ .

- 1. Select appropriate stochastic and deterministic basis, i.e.,  $\{\psi_i(\xi)\}_{i=1}^p$  and  $\{\varphi_j(x)\}_{i=1}^m$ .
- 2. Generate simulation outputs  $\{u(x_i, \xi_j)\}_{i=1,j=1}^{m}$  associated with given collocation points. 3. Arrange the system (2) into a vector form (7), and solve the BP denoising problem

$$\operatorname{vec}(\hat{\mathbf{c}}) = \underset{\operatorname{vec}(\hat{\mathbf{c}})}{\operatorname{arg\,min}} \| \operatorname{vec}(\hat{\mathbf{c}}) \|_1 \quad \text{subject to} \quad \| \operatorname{vec}(\mathbf{u}) - \mathbf{\Theta} \operatorname{vec}(\hat{\mathbf{c}}) \|_2 \le \epsilon = 10^{-7},$$

where  $\Theta = I_m \otimes \Psi$ , then reconstruct the solution  $u(x, \xi)$  with coefficients  $\hat{\mathbf{c}}$ , i.e.,

$$\hat{u}(x,\xi) = \sum_{i=1}^{p} \sum_{i=1}^{m} \hat{c}_{ij} \varphi_{j}(x) \psi_{i}(\xi).$$

4. Compute the covariance function  $Cov_{\hat{u}}(x, x')$  by the definition (12).

**Remark 1.** By using the multivariate Legendre polynomials  $\{\psi_i(\xi)\}_{i=1}^p$ , we can rewrite the above result as follows:

$$\hat{u}(x,\xi) = \sum_{i=1}^{m} \hat{c}_{1j}\varphi_{j}(x) + \sum_{i=2}^{p} \sum_{i=1}^{m} \hat{c}_{ij}\varphi_{j}(x)\psi_{i}(\xi) = E_{\hat{u}}(x) + \sum_{i=2}^{p} \sum_{i=1}^{m} \hat{c}_{ij}\varphi_{j}(x)\psi_{i}(\xi).$$
(13)

Therefore, the approximation of covariance function  $Cov_{\mu}(x, x')$  has the form

$$\operatorname{Cov}_{\hat{u}}(x, x') = \sum_{i=2}^{p} \left( \sum_{j=1}^{m} \hat{c}_{ij} \varphi_{j}(x) \right) \left( \sum_{j'=1}^{m} \hat{c}_{ij'} \varphi_{j'}(x') \right). \tag{14}$$

Remark 2. Instead of the matrix form (2), the constraint of BP problem (8) is written in a vector form for the ease of theoretical analysis throughout this paper, which is not necessary for numerical implementation. In other words, one can directly solve the BP denoising problem in Algorithm 1 with constraint in a matrix form, i.e.,  $\|\mathbf{u} - \mathbf{v}\mathbf{c}\mathbf{\Phi}\|_2 \le \epsilon$ .

#### 3.2. Karhunen-Loève basis extraction

Instead of using the standard finite element basis for the sparse representation of  $u(x, \xi)$  in the spatial domain, we adopt a data-driven basis extracted from KL analysis (3), in which the kernel function is generated from Algorithm 1.

Let  $\mathcal{T}_h$  be a triangulation of D parametrized with a mesh size h > 0 and grid points  $\{x_j\}_{j=1}^m$ , and let  $V_h = \text{span}\{\varphi_1(x), \dots, \varphi_m(x)\}$  denote the finite element space associated with  $\mathcal{T}_h$ . Given the covariance kernel function  $\text{Cov}_{\hat{u}}(x, x')$ , the finite element approximation of the KL integral equation (3) has the form: find  $\lambda_j \in \mathbb{R}_+$  and  $0 \neq \phi_j(x) \in V_h$  such that

$$\int_{D} \left( \int_{D} \operatorname{Cov}_{\hat{u}}(x, x') \phi_{j}(x') \, dx' \right) \nu(x) \, dx = \lambda_{j} \int_{D} \phi_{j}(x) \nu(x) \, dx \text{ for all } \nu(x) \in V_{h}.$$
(15)

Specifically, we assume that  $\phi_j(x) \in V_h$  and  $\phi_j(x) = \sum_{k=1}^m \mu_j^{(k)} \varphi_k(x)$  for j = 1, ..., m. Then, the problem (15) turns out to be a generalized eigenvalue problem [21]

$$\mathbf{C}\mu_{j} = \lambda_{j}\mathbf{M}\mu_{j} \quad \text{for } j = 1, \dots, m, \tag{16}$$

where the generalized eigenvectors  $\{\mu_j\}$  are given by  $\mu_j = \left(\mu_j^{(1)}, \dots, \mu_j^{(m)}\right)^T$ , and matrices

$$\mathbf{C} = \left( \int_{D \times D} \mathsf{Cov}_{\hat{u}}(x, x') \varphi_i(x') \varphi_j(x) \, dx' dx \right)_{i, j = 1}^m \quad \text{and} \quad \mathbf{M} = \left( \int_{D} \varphi_i(x) \varphi_j(x) \, dx \right)_{i, j = 1}^m$$

are both symmetric positive definite. Without loss of generality, the non-negative eigenvalues  $\{\lambda_j\}_{j=1}^m$  are arranged in decreasing order with eigenvectors assumed to be  $\mathbf{M}$ -orthonormal, i.e.,  $\mathbf{\Phi}\mathbf{M}\mathbf{\Phi}^T = \mathbf{I}_m$  where  $\mathbf{I}_m$  is an  $m \times m$  identity matrix and  $\mathbf{\Phi} = (\mu_1, \dots, \mu_m)^T$  (not relabeled).

To show the effectiveness of such a basis, we consider first of all the projection of expansion (13) into the subspace spanned by the eigenfunctions  $\{\phi_j(x)\}_{j=1}^m$ , that is,

$$\hat{u}(x,\xi) = \sum_{j=1}^{m} \langle \hat{u}(x,\xi), \phi_j(x) \rangle \phi_j(x) = \sum_{i=1}^{p} \sum_{j=1}^{m} \check{c}_{ij} \phi_j(x) \psi_i(\xi) := \check{u}(x,\xi),$$
(17)

where  $\langle \cdot, \cdot \rangle$  denotes the  $L^2(D)$  inner product. By the orthonormality condition of basis functions  $\{\psi_i(\xi)\}_{i=1}^p$ , it can be easily deduced from (17) that

$$\sum_{j=1}^{m} \hat{c}_{ij} \varphi_j(x) = \sum_{j=1}^{m} \check{c}_{ij} \varphi_j(x) \text{ for } 1 \le i \le p.$$

$$\tag{18}$$

Then, by evaluating (18) at the given set of grid points  $\{x_j\}_{j=1}^m$ , we arrive at the equality

 $\hat{\mathbf{c}} \mathbf{I}_m = \check{\mathbf{c}} \mathbf{\Phi}$  or, equivalently,  $\check{\mathbf{c}} = \hat{\mathbf{c}} \mathbf{\Phi}^{-1}$ 

where  $\check{\mathbf{c}} = (\check{c}_{ij})$  is the coefficient matrix, which provides us with an algorithm for the construction of  $\check{u}(x, \xi)$ .

# **Algorithm 2** Optimal projection-based sparse representation.

**Input**: stochastic and spatial collocation points, namely,  $\{\xi_i\}_{i=1}^n$  and  $\{x_j\}_{j=1}^m$ .

**Output**: sparse coefficients  $\check{\mathbf{c}} = (\check{c}_{ij})$  via optimal projection.

- 1. Recover the solution (13) and its covariance (14) using Algorithm 1.
- 2. Solve the KL eigenvalue problem (15) to obtain the data-driven basis  $\{\phi_i(x)\}_{i=1}^m$ .
- 3. Assemble the projection matrix  $\Phi = (\phi_i(x_i))$  and reconstruct the solution  $u(x, \xi)$  by

$$\check{u}(x,\xi) = \sum_{i=1}^{p} \sum_{j=1}^{m} \check{c}_{ij} \phi_j(x) \psi_i(\xi),$$

where the expansion coefficients are determined by  $\check{\mathbf{c}} = \hat{\mathbf{c}} \Phi^{-1}$ .

Now we are ready to show the enhancement of sparsity in representing  $u(x, \xi)$  via Algorithm 2. An estimation on the expansion coefficients is presented below. Its proof is standard and is given in the Appendix A for reference.

**Theorem 3.** The coefficients of expansion  $\check{u}(x, \xi)$  satisfy the estimation

$$\sum_{i=2}^{p} |\check{c}_{ij}|^2 = \lambda_j \text{ for } j = 1, \dots, m,$$
(19)

where  $\lambda_i$  is the j-th eigenvalue of the problem (15). Moreover, the expansion (17) satisfies the equality

$$\mathbb{E}\left[\int_{D} \left(\check{u}(x,\xi) - E_{\check{u}}(x)\right)^{2} dx\right] = \sum_{j=1}^{m} \lambda_{j} \text{ where } E_{\check{u}}(x) = \sum_{j=1}^{m} \check{c}_{1j}\phi_{j}(x). \tag{20}$$

Due to the fast decay of eigenvalues in many applications [16], Theorem 3 implies that the expansion coefficients associated with small eigenvalues can be compressed into the region close to zero, and hence could be negligible. This enables us to further increase the sparsity of expansion (17). Such a technique, also known as the principle component analysis (PCA) in statistics or proper orthogonal decomposition (POD) in reduced-order modeling [6–8,12], may reward the basis functions with small coefficient values. Consequently, the proposed DCS method may provide a more attractive alternative to the stochastic problem (1) (see Section 4 for more details).

## 3.3. Optimality of data-driven basis

We now illustrate the optimal property of our data-driven basis, *i.e.*, the projection of sample simulations onto the space spanned by that basis is the best approximation among all such orthogonal functions in  $L^2(D)$ .

Since one is usually interested in the deviations about a mean value, modified sample observations are constructed by  $v(x, \xi_i) = v(x, \xi_i) - E_{\hat{u}}(x)$ ,  $1 \le i \le n$ , where the expectation is approximated by  $E_{\hat{u}}(x)$ . We then have the following result on the data-driven basis whose proof involves standard techniques, see Appendix B.

**Theorem 4.** Given the modified sample observations, the basis  $\{\phi_j(x)\}_{j=1}^m$  minimizes, among all orthogonal basis functions of dimension m, the projective error

$$\mathcal{J}(\phi_1,\ldots,\phi_m) = \frac{1}{n} \sum_{i=1}^n \mathbb{E} \left[ \| v(x,\xi_i) - \sum_{k=1}^m \left\langle v(x,\xi_i), \phi_k \right\rangle \phi_k \|^2 \right], \tag{21}$$

where  $\langle \cdot, \cdot \rangle$  and  $\| \cdot \|$  denote the  $L^2(D)$  inner product and norm, respectively.

As can be seen from Theorem 4, the data-driven basis captures the essential information in the sample measurements. It is therefore more promising than the standard finite element basis in exploiting the sparse modes of the solution  $u(x, \xi)$ . Moreover, the dominant solution patterns in the  $\ell_2$ -norm sense could also be of crucial importance in the  $\ell_1$ -norm sense, and the details are presented in the following section.

## 4. Compressive sensing with data-driven basis

Instead of representing  $u(x, \xi)$  through the optimal projection, a convexified  $\ell_1$ -norm minimization problem associated with our data-driven basis is proposed in this section. A detailed analysis is presented to show the effectiveness of our DCS method, together with a multi-fidelity algorithm in the numerical implementation.

We recall that the proposed sparse recovery procedure is defined by

$$\operatorname{vec}(\tilde{\mathbf{c}}) = \underset{\operatorname{vec}(\mathbf{c})}{\operatorname{arg\,min}} \| \operatorname{vec}(\mathbf{c}) \|_{1} \text{ subject to } \operatorname{vec}(\mathbf{u} \mathbf{M}^{\frac{1}{2}}) = \left( \left( \mathbf{\Phi} \mathbf{M}^{\frac{1}{2}} \right)^{T} \otimes \mathbf{\Psi} \right) \operatorname{vec}(\mathbf{c}), \tag{22}$$

where the symmetric and positive definite mass matrix  $\mathbf{M}$  has the eigendecomposition  $\mathbf{M} = \mathbf{M}^{\frac{1}{2}} (\mathbf{M}^{\frac{1}{2}})^T$ .

Meanwhile, one fundamental premise of the DCS method is that the information matrix satisfies certain requirements on the RIP constant. To show this, we recall the M-orthonormal condition of eigenvectors in (16), that is,

$$I = \Phi M \Phi^{T} = \Phi M^{\frac{1}{2}} \left( \Phi M^{\frac{1}{2}} \right)^{T}. \tag{23}$$

Then, by Lemma 1 and (23), it immediately implies that

$$\delta_{S}\left(\left(\mathbf{\Phi}\mathbf{M}^{\frac{1}{2}}\right)^{T}\otimes\mathbf{\Psi}\right)=\delta_{S}(\mathbf{\Psi}),\tag{24}$$

i.e., the RIP constant of DCS method remains the same as the standard CS setting.

On the other hand, the representations (4) and (17) are expressed w.r.t. the same basis functions but with different coefficient values. In fact, the coefficients with relatively large values stay the same in both cases, while the expansion coefficients with relatively small values can be further compressed through the BP problem (22). Compared with the conventional CS methods, our DCS approach can significantly increase the sparsity of expansion coefficients without changing the value of RIP constant. Consequently, the associated recovery accuracy can be further improved, which can be highly desirable in practice. Moreover, the number of energetically dominant solution modes does not vary substantially as the mesh size h gets refined, i.e., the eigenpair approximation error can be bounded in terms of the mesh spacing [21]. This allows us to use the low-fidelity simulations, e.g., solutions on coarse meshes, for the recovery of covariance kernel function with acceptable accuracy and at low cost. Then, the data-driven basis can be constructed for the representation of high-fidelity models, e.g., solutions on fine meshes. The algorithm for such an efficient sparse recovery procedure using multi-fidelity data is given below.

#### Algorithm 3 Multi-fidelity compressive sensing with data-driven basis.

**Input**: coarse and fine mesh sizes (H and h, respectively), stochastic collocation points.

**Output**: compressed coefficients  $\tilde{\mathbf{c}} = (\tilde{c}_{ij})$  w.r.t. data-driven basis for high-fidelity representation.

- 1. Generate coarse mesh sample simulations and use Algorithm 1 to recover the covariance function (14).
- 2. Solve the problem (15) to obtain the data-driven basis  $\{\phi_j(x)\}_{i=1}^m$  on the fine mesh, then construct the matrix  $\Phi = (\phi_i(x_j))$ .
- 3. Generate fine mesh sample simulations and solve the corresponding BP denoising problem

$$\operatorname{vec}(\tilde{\mathbf{c}}) = \underset{\operatorname{vec}(\mathbf{c})}{\operatorname{arg\,min}} \| \operatorname{vec}(\mathbf{c}) \|_1 \quad \text{subject to} \quad \| \operatorname{vec}(\mathbf{u}) - \mathbf{\Theta} \operatorname{vec}(\mathbf{c}) \|_2 \le \epsilon = 10^{-7},$$

where  $\Theta = \Phi_m^T \otimes \Psi$ , then reconstruct the solution  $u(x, \xi)$  with coefficients  $\tilde{\mathbf{c}}$ , *i.e.*,

$$\tilde{u}(x,\xi) = \sum_{i=1}^{p} \sum_{j=1}^{m} \tilde{c}_{ij} \phi_j(x) \psi_i(\xi).$$

Note that the constraint equation in (22) and the linear system (2) are equivalent up to a linear transformation, and the representation of solution now has the form (4). Numerical results are reported in the following section to verify the effectiveness of our DCS method.

## 5. Numerical experiments

In this section, numerical experiments are reported to show the effectiveness of our DCS method. First, an explicit function with high compressibility is considered to demonstrate the accuracy of our covariance recovery strategy, *i.e.*, the Algorithm 1. Then, the numerical results on a second-order elliptic boundary value problem with stochastic inputs are presented to demonstrate the efficiency of our DCS approach for recovering the sparse solution globally over the physical domain.

### 5.1. Example with high compressibility

We consider a highly compressible function,

$$u(x, \boldsymbol{\xi}) = \sum_{i=1}^{d} \ell_0(\xi_i) + (e^x - 1) \sum_{i=1}^{d} \ell_1(\xi_i) + (e^{1-x} - 1) \sum_{i=1}^{d} \ell_2(\xi_i)$$
(25)

where x is over the interval D = [0, 1], random variables  $\{\xi_i\}_{i=1}^d$  are assumed to be independently and uniformly distributed on [-1, 1], and  $\ell_j(\xi)$  represents the j-th order univariate Legendre polynomial. In particular, by choosing d = 21, the covariance function has an explicit expression

$$Cov_{u}(x, x') = 7(e^{x} - 1)(e^{x'} - 1) + \frac{21}{5}(e^{1 - x} - 1)(e^{1 - x'} - 1).$$
(26)

Next, given the random inputs  $\{\xi_i\}_{i=1}^n$  and spatial collocation points  $\{x_j = (j-1)/2^5\}_{j=1}^m$  where m = 33, Algorithm 1 is applied to recover the covariance function (14) in which the recovery result is denoted by  $\text{Cov}^{\text{CS}}(x, x')$ . Here, the standard continuous piecewise linear finite element basis and the 2nd-order Legendre PC basis are used in the numerical implementation. Meanwhile, using the same sample simulations  $\{u(x, \xi_i)\}_{i=1}^n$ , the conventional MC approach is applied for comparison purpose, namely,

$$Cov^{MC}(x, x') = \frac{1}{n} \sum_{i=1}^{n} u(x, \xi_i) u(x', \xi_i) - \left(\frac{1}{n} \sum_{i=1}^{n} u(x, \xi_i)\right) \left(\frac{1}{n} \sum_{i=1}^{n} u(x', \xi_i)\right).$$

To show the efficiency of the proposed covariance recovery method, the error estimate associated with approximating (26) by  $Cov^{CS}(x, x')$  and  $Cov^{MC}(x, x')$  is presented in Table 1 and Fig. 1, where different sample sizes are used for the recovery,  $err^{MC} := \| Cov^{MC} - Cov_u \|_{L^2(D \times D)}$  and  $err^{CS} := \| Cov^{CS} - Cov_u \|_{L^2(D \times D)}$ .

As shown in Table 1 and Fig. 1, the MC approach converges slowly with order 0.47, that is,  $err^{MC} \approx \mathcal{O}(n^{-1/2})$ , and fails to provide accurate statistical moments especially with a limited number of sample observations. However, such a highly "incomplete" set of random observations does contain enough information for the accurate recovery of covariance function.

**Table 1**Error estimates for covariance recovery using MC and CS methods.

n (sample size)	40	60	80	100	120	125	130	135	140	160	order
err <sup>MC</sup> ×10 <sup>-2</sup>	3.53	2.76	2.47	2.17	2.13	2.02	1.97	1.92	1.88	1.82	0.47
$err^{CS} \times 10^{-2}$	64.97	61.21	48.55	26.00	15.70	8.24	2.29	0.03	0.03	0.03	-

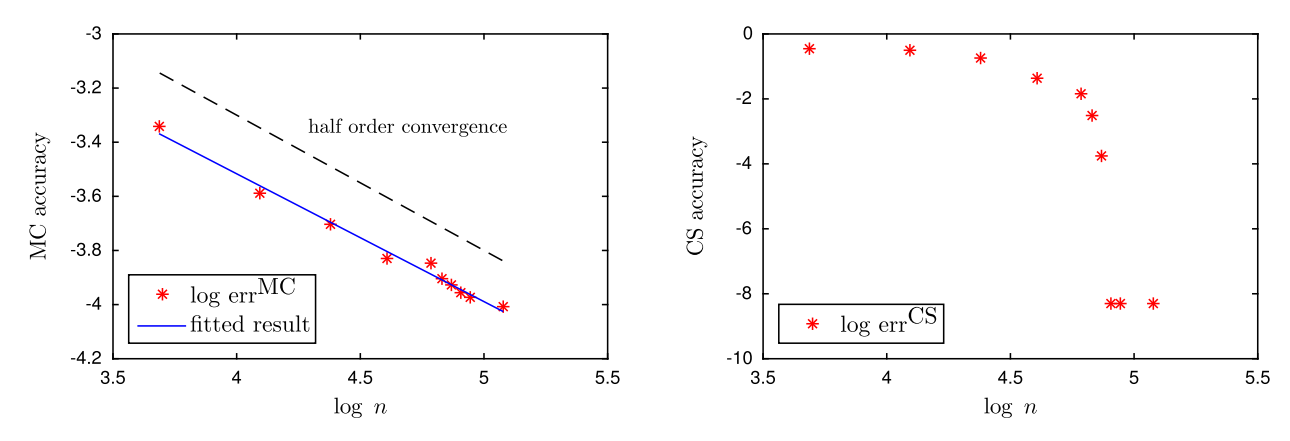


Fig. 1. Error estimates for covariance recovery by MC and CS methods w.r.t. different sample sizes.

Specifically, the right figure implies that high accuracy can be achieved from far fewer samples than required by the MC method. This ensures the effectiveness of the data-driven basis that plays a key role in our DCS method.

In particular, our proposed covariance recovery strategy remains valid for mesh refinement, *i.e.*, the number of measurements required for accurate recovery remains almost constant as the mesh gets refined, which enables us to construct data-driven basis via low-fidelity simulations at low cost. Such a property is highly desirable for the representation of high-fidelity solutions, and the details are presented in the following section.

# 5.2. Applications to uncertainty quantification

We now consider a one-dimensional elliptic boundary value problem with random inputs, which has been studied in earlier works on uncertainty quantification and stochastic models [1,22]. The problem is given by

$$\begin{cases}
-\nabla \cdot (a(x, \xi)\nabla u(x, \xi)) = f(x) & \text{in } D = (0, 1), \\
u(x, \xi) = 0 & \text{on } \partial D,
\end{cases}$$
(27)

where  $f(x) = \sin(\pi x)$ , and the stochastic coefficient field  $a(x, \xi) = a(x, \xi_1, \dots, \xi_d)$  takes on the form

$$a(x, \boldsymbol{\xi}) = E_a(x) + \sigma \sum_{j=1}^d \sqrt{\lambda_j} \,\vartheta_j(x) \,\xi_j. \tag{28}$$

Here,  $E_a(x)$  denotes the mean value of the diffusion coefficient,  $\sigma > 0$  is an amplification factor,  $\{\xi_j\}_{j=1}^d$  are sampled independently and uniformly at random from the set of outcomes [-1,1], and  $\{(\lambda_j,\vartheta_j)\}_{j=1}^d$  are defined by the first  $d \in \mathbb{Z}_+$  eigenpairs of the KL eigenvalue problem (15) with an exponential kernel function

$$Cov_{aa}(x, x') = \exp\left(-\frac{|x - x'|}{l_c}\right),\tag{29}$$

where the correlation length  $l_c > 0$  is typically used to characterize the decay of eigenvalues.

Without loss of generality, we choose the mean value  $E_a(x) = 1$ , the amplification factor  $\sigma = 0.5$ , the dimension of random inputs d = 19, and the correlation length  $l_c = 0.2$  so that the coefficient (28) is uniform coercive. Moreover, let D = [0, 1] be uniformly divided into several disjoint intervals with mesh size h > 0, the linear finite element basis and the 2nd-order Legendre polynomial functions are utilized for numerical discretization.

# 5.2.1. Robustness of data-driven basis

To show the efficiency of Algorithm 3, numerical results are reported in this section to demonstrate the robustness of sparse modes as the spatial resolution increases. That is, with the number of model simulations staying fixed, the set of energetically dominant solution patterns does not show substantial variations as the mesh gets refined.

For illustration, we choose  $h = 2^{-6}$  and  $2^{-8}$  (i.e., m = 65 and 257 respectively), n = 60 independent sample simulations of problem (27) are used for the sparse recovery of (12) via Algorithm 1. By solving the KL eigenvalue problem (15), Fig. 2 depicts the largest 40 eigenvalues and their cumulative energy ratios (defined as

$$\rho_k := \sum_{j=1}^k \lambda_j / \sum_{j=1}^m \lambda_j,$$

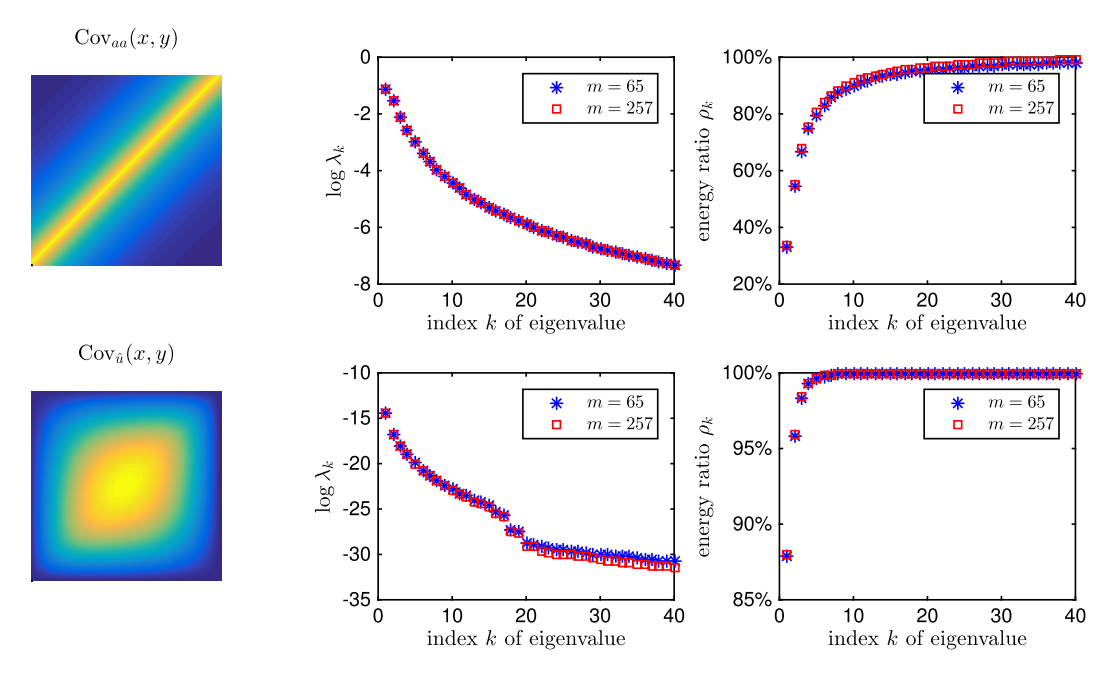


Fig. 2. Covariance, spectrum and energy ratio for coefficient (1st row) and solution (2nd row).

for k = 1, 2, ..., m), as well as the covariance functions of coefficient  $a(x, \xi)$  and numerical solution  $\hat{u}(x, \xi)$ . Roughly speaking, the cumulative energy ratio  $\rho_k$  measures the "information content" of the sample observations captured by the first k terms in our data-driven basis.

The results in Fig. 2 show that the distribution of spectrum remains almost unchanged as the mesh gets refined. Therefore, it is possible to utilize the low-cost coarse mesh (low-fidelity) sample simulations to have fast generation of fine scale (high-fidelity) data-driven basis functions with little loss in accuracy. This key observation ensures the effectiveness of our multi-fidelity DCS algorithm.

# 5.2.2. Improvement of sparsity and accuracy

Given the coarse and fine mesh parameters, say,  $H = 2^{-6}$  and  $h = 2^{-8}$  respectively, we apply Algorithm 1 with n = 60 sample simulations on the coarse mesh for the recovery of covariance function  $Cov_{\hat{u}}(x, x')$ . The eigenvalues and the corresponding cumulative energy ratios are depicted in Fig. 2. On the other hand, only n = 60 sample simulations are generated on fine mesh for the recovery of high-fidelity solution.

From Fig. 2 we see that in order to obtain, say, 99.99% energy of  $\hat{u}(x,\xi)$  via the KL expansion, only 12 terms are needed. This immediately implies that Algorithm 2 can be used to compress the expansion coefficients of (1). Without loss of generality, we consider the coefficients with absolute values larger than a fixed threshold  $\tau = 1 \times 10^{-7}$ . Consequently, by (19), the coefficients associated with the eigenvalues less than  $\tau^2 p \approx 2.1 \times 10^{-12} \approx \lambda_{60}$  are of little importance and omitted in what follows.

By using the conventional CS method, projection-based method (*i.e.*, Algorithm 2) and DCS method (*i.e.*, Algorithm 3) respectively, the corresponding sparse recovery results  $\hat{\mathbf{c}}$ ,  $\check{\mathbf{c}}$  and  $\check{\mathbf{c}}$  are depicted in Fig. 3, in which the matrix entries with absolute values larger than the given threshold value  $\tau = 1 \times 10^{-7}$  are marked in blue color. The statistical results are reported in Table 2, where the total degree of freedoms (DoFs) in this example is  $m \times p = 257 \times 210 = 53970$ .

Before presenting the quantitative results, several observations can be drawn from Fig. 3: (i) when the conventional CS method is applied for recovery, different spatial points show different sparse patterns, hence there are a moderate number of coefficients that contribute to the representation of solution as depicted in the first picture; (ii) due to the spectrum decay, it can be found in the second picture that the coefficients associated with the last m - 60 = 197 eigenfunctions can be compressed, which validates our estimate (19); (iii) the third picture shows that our DCS performs better than other two methods, where the sparsity is further enhanced by applying the  $\ell_1$ -norm minimization technique.

We now present the quantitative analysis on the statements above. By choosing a sequence of threshold values  $\{\tau=10^{-1-i}\}_{i=1}^7$ , the statistical results on the sparsity of different recovery methods are given in Table 2. Meanwhile, the relative error estimations associated with approximating the expectation  $\mathbb{E}[u_h]$  and variance  $\mathbb{V}[u_h]$  by the CS method, Algorithm 2 and Algorithm 3 are presented in Table 3. Here, the reference solutions  $\mathbb{E}[u_h]$  and  $\mathbb{V}[u_h]$  are computed by the standard MC finite element method with 4000 sample simulations.

To recover the fine-mesh solutions, Fig. 3 and Table 3 imply that both the sparsity and the approximation accuracy are improved by our DCS method. Specifically,  $\check{\mathbf{c}}$  is sparser than  $\hat{\mathbf{c}}$  for all threshold values  $\{\tau=10^{-1-\hat{i}}\}_{\hat{i}=1}^7$  due to the fast decay of eigenvalues, while  $\check{\mathbf{c}}$  is sparser than  $\check{\mathbf{c}}$ , provided that  $\tau$  is sufficient small. This is because that the primary solution modes,

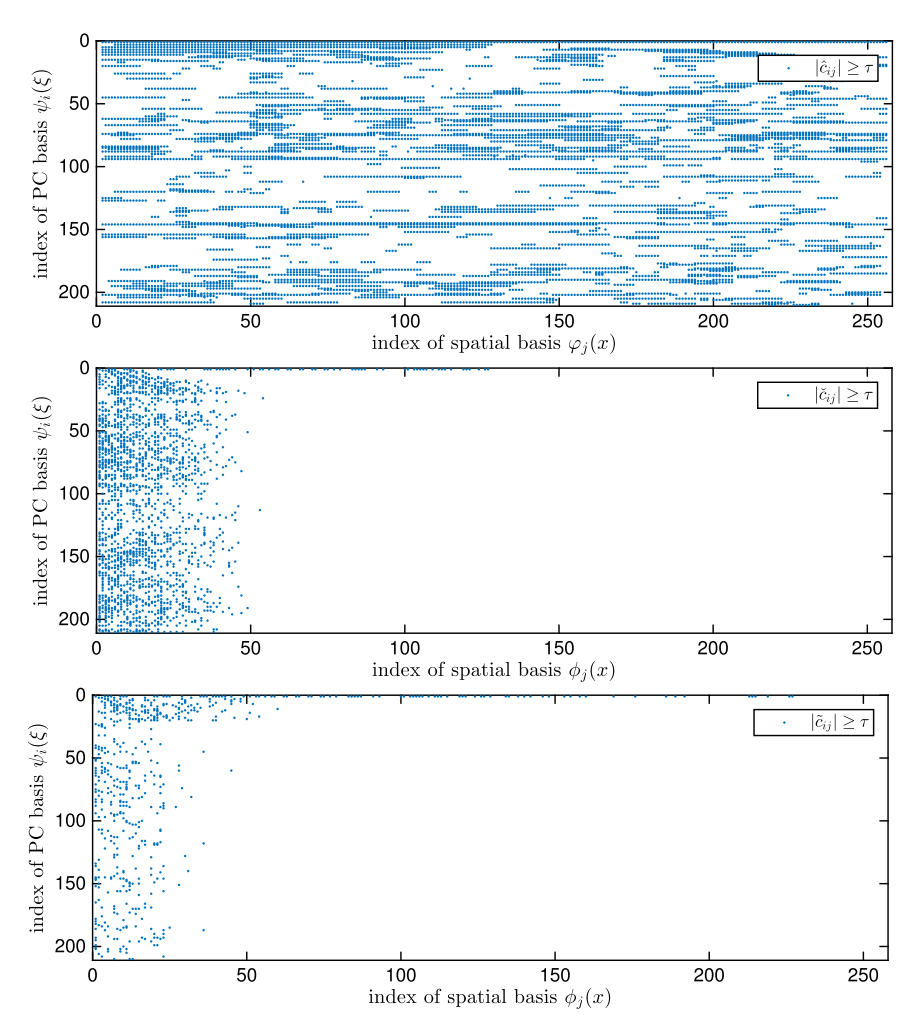


Fig. 3. Entries in coefficient matrices  $\hat{\mathbf{c}}$ ,  $\check{\mathbf{c}}$  and  $\check{\mathbf{c}}$  with absolute values larger than  $\tau=1\times10^{-7}$ . (For interpretation of the colors in the figure(s), the reader is referred to the web version of this article.)

**Table 2**Sparsity w.r.t. different methods and threshold values.

	$\#\{ \hat{\mathbf{c}}_{ij}  \geq \tau\}$	$\left(\frac{\#\{ \hat{\mathbf{c}}_{ij}  \geq \tau\}}{DoFs}\right)$	$\#\{ \check{\mathbf{c}}_{ij}  \geq \tau\}$	$\left(\frac{\#\{ \check{\mathbf{c}}_{ij}  \geq \tau\}}{DoFs}\right)$	$\#\{ \tilde{\mathbf{c}}_{ij}  \geq \tau\}$	$\left(\frac{\#\{ \tilde{\mathbf{c}}_{ij}  \geq \tau\}}{DoFs}\right)$
$ au = 10^{-2}$	239	(0.443%)	1	(0.002%)	1	(0.002%)
$\tau = 10^{-3}$	255	(0.472%)	2	(0.004%)	2	(0.004%)
$ au = 10^{-4}$	1113	(2.062%)	19	(0.035%)	19	(0.035%)
$\tau = 10^{-5}$	2571	(4.764%)	61	(0.113%)	64	(0.119%)
$\tau = 10^{-6}$	11665	(21.614%)	328	(0.608%)	321	(0.428%)
$\tau = 10^{-7}$	18042	(33.430%)	3760	(6.967%)	1155	(2.140%)
$\tau = 10^{-8}$	29692	(55.016%)	13743	(25.464%)	3109	(5.761%)

 Table 3

 Error estimates associated with approximating statistic moments.

	$u = \hat{u}$	$u = \check{u}$	$u = \tilde{u}$		$u = \hat{u}$	$u = \check{u}$	$u = \tilde{u}$
$\frac{\ \mathbb{E}[u_h] - \mathbb{E}[u]\ _{L^2(D)}}{\ \mathbb{E}[u_h]\ _{L^2(D)}} \times 10^{-4}$	3.158	3.158	1.607	$\frac{\ \mathbb{V}[u_h] - \mathbb{V}[u]\ _{L^2(D)}}{\ \mathbb{V}[u_h]\ _{L^2(D)}} \times 10^{-2}$	1.793	1.793	0.839

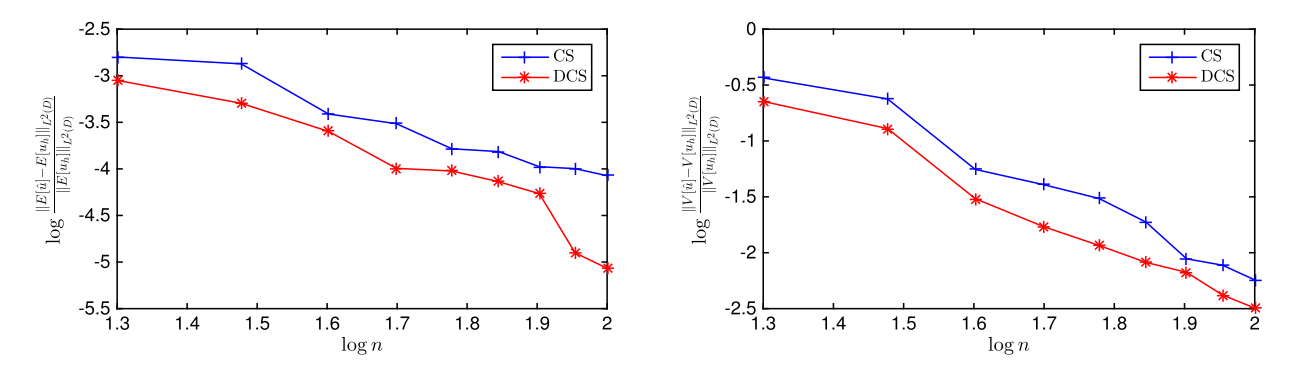


Fig. 4. Error estimates associated with approximating statistic moments w.r.t. different sample sizes (n).

 Table 4

 Error estimates associated with approximating expectation w.r.t. different sample sizes.

Number of samples	20	30	40	50	60	70	80	90
$\frac{\ \mathbb{E}[\hat{u}] - \mathbb{E}[u_h]\ _{L^2(D)}}{\ \mathbb{E}[u_h]\ _{L^2(D)}} \times 10^{-4}$	15.89	13.41	3.88	3.06	1.65	1.53	1.06	1.01
$\frac{\ \mathbb{E}[\tilde{u}] - \mathbb{E}[u_h]\ _{L^2(D)}}{\ \mathbb{E}[u_h]\ _{L^2(D)}} \times 10^{-4}$	8.89	5.06	2.53	1.01	0.95	0.73	0.54	0.16

 Table 5

 Error estimates associated with approximating covariance w.r.t. different sample sizes.

Number of samples	20	30	40	50	60	70	80	90
$\frac{\ \mathbb{V}[\hat{u}] - \mathbb{V}[u_h]\ _{L^2(D)}}{\ \mathbb{V}[u_h]\ _{L^2(D)}} \times 10^{-2}$	36.58	23.77	5.56	4.07	3.06	1.88	0.88	0.77
$\frac{\ \mathbb{V}[\tilde{u}] - \mathbb{V}[u_h]\ _{L^2(D)}}{\ \mathbb{V}[u_h]\ _{L^2(D)}} \times 10^{-2}$	22.51	12.90	3.04	1.72	1.16	0.82	0.67	0.42

or, to put it differently, the basis functions with relatively large coefficients, are most important for both the representations (4) and (17). On the other hand, the basis functions with small coefficients are compressed by carrying out Algorithm 3, which further enhances the sparsity of representation (4).

Next, to further illustrate the advantages of DCS method as the number of high-fidelity sample simulations varies, we test the conventional CS method and the proposed DCS method with fixed mesh spacing but varying sample size. The computational results are given in Table 4 and Table 5. Clearly, the recovery accuracy is improved using our DCS method as depicted in Fig. 4, which validates the claims given earlier.

#### 5.2.3. Robustness of DCS method

Now we are ready to illustrate the advantages of DCS method as both the mesh spacing and the number of high-fidelity observations change.

To be specific, we consider first the varying mesh sizes, where the sample size n = 60 is fixed for both the low- and high-fidelity simulations. To recover the fine-scale solution with mesh sizes  $\{h_i = 2^{-9+i}\}_{i=1}^3$ , the coarse meshes with  $\{H_i = 2^{-8+i}\}_{i=1}^3$  are adopted respectively. The compositions of expansion coefficient w.r.t. different methods are then given in Table 7, and the corresponding relative errors are presented in Table 6.

The component ratio  $\rho(\tau) = \#\{|\mathbf{c}_{ij}| \geq \tau\}$ /DoFs, which roughly characterizes the sparsity of the recovered coefficients  $\mathbf{c}$ , is summarized in Table 7 and shown in Fig. 5 for different methods  $\hat{\mathbf{c}}$ ,  $\check{\mathbf{c}}$  and  $\check{\mathbf{c}}$ . Note that, by Table 7, the coefficients associated with our data-driven basis are significantly compressed when compared with the conventional CS method. Moreover, the dominant sparse patterns for Algorithm 2 and Algorithm 3 remain almost identical as the mesh gets refined, while the less important solution modes can be further compressed via the DCS method (e.g., the number  $\#\{10^{-7} \leq |\mathbf{c}_{ij}| < 10^{-6}\}$  in Table 7).

Next, we consider the situation where both the sample size and mesh spacing change, and the results are depicted in Fig. 6. Note that, as the mesh gets refined, recovery accuracies for both the CS and DCS methods are improved. Clearly, like the previous case, our DCS method performs better than the conventional CS method.

To sum up, the numerical results given in section 5 demonstrate that the proposed DCS method can significantly enhance the sparsity of expansion coefficients and accurately recover the sparse solution at low cost.

 Table 6

 Error estimates associated with approximating statistic moments.

h	$2^{-6}$	$2^{-7}$	$2^{-8}$	h	$2^{-6}$	$2^{-7}$	$2^{-8}$
$\frac{\ \mathbb{E}[\hat{u}] - \mathbb{E}[u_h]\ _{L^2(D)}}{\ \mathbb{E}[u_h]\ _{L^2(D)}} \times 10^{-4}$	7.00	5.98	3.16	$\frac{\ \mathbb{V}[\hat{u}] - \mathbb{V}[u_h]\ _{L^2(D)}}{\ \mathbb{V}[u_h]\ _{L^2(D)}} \times 10^{-2}$	2.66	2.26	1.79
$\frac{\ \mathbb{E}[\check{u}] - \mathbb{E}[u_h]\ _{L^2(D)}}{\ \mathbb{E}[u_h]\ _{L^2(D)}} \times 10^{-4}$	7.00	5.98	3.16	$\frac{\ \mathbb{V}[\check{u}] - \mathbb{V}[u_h]\ _{L^2(D)}}{\ \mathbb{V}[u_h]\ _{L^2(D)}} \times 10^{-2}$	2.66	2.26	1.79
$\frac{\ \mathbb{E}[\tilde{u}] - \mathbb{E}[u_h]\ _{L^2(D)}}{\ \mathbb{E}[u_h]\ _{L^2(D)}} \times 10^{-4}$	4.19	3.51	1.61	$\frac{\ \mathbb{V}[\tilde{u}] - \mathbb{V}[u_h]\ _{L^2(D)}}{\ \mathbb{V}[u_h]\ _{L^2(D)}} \times 10^{-2}$	1.59	1.13	0.88

**Table 7**Sparsity w.r.t. different methods, threshold values and mesh sizes.

h (DoFs)		$2^{-6}$	(13650)	$2^{-7}$	(27090)	$2^{-8}$	(53970)
	$\tau = 10^{-3}$	103	(0.755%)	176	(0.650%)	255	(0.472%)
$(\#\{ \hat{\mathbf{c}}_{\cdot\cdot}  > \tau\})$	$\tau = 10^{-4}$	384	(2.549%)	625	(2.307%)	1113	(2.062%)
$\#\{ \hat{\mathbf{c}}_{ij}  \geq \tau\}  \left(\frac{\#\{ \hat{\mathbf{c}}_{ij}  \geq \tau\}}{\text{DoFs}}\right)$	$\tau = 10^{-5}$	961	(7.040%)	1570	(5.795%)	2571	(4.764%)
DOFS )	$\tau = 10^{-6}$	3412	(26.476%)	6143	(22.676%)	11665	(21.614%)
	$\tau = 10^{-7}$	4816	(35.282%)	9778	(36.094%)	18042	(33.430%)
	$\tau = 10^{-3}$	3	(0.022%)	2	(0.007%)	2	(0.004%)
v	$\tau = 10^{-4}$	13	(0.095%)	14	(0.052%)	19	(0.035%)
$\#\{ \check{\mathbf{c}}_{ij}  \geq \tau\}  \left(\frac{\#\{ \mathbf{c}_{ij}  \geq \tau\}}{DoFs}\right)$	$\tau = 10^{-5}$	57	(0.418%)	58	(0.214%)	61	(0.113%)
DoFs )	$\tau = 10^{-6}$	449	(3.289%)	370	(1.366%)	328	(0.608%)
	$\tau = 10^{-7}$	3961	(29.018%)	3663	(14.692%)	3760	(6.967%)
	$\tau = 10^{-3}$	3	(0.022%)	2	(0.007%)	2	(0.004%)
( 407 )	$\tau = 10^{-4}$	13	(0.095%)	14	(0.052%)	19	(0.035%)
$\#\{ \tilde{\mathbf{c}}_{ij}  \geq \tau\}  \left(\frac{\#\{ \tilde{\mathbf{c}}_{ij}  \geq \tau\}}{DoFs}\right)$	$\tau = 10^{-5}$	60	(0.440%)	60	(0.221%)	64	(0.119%)
DoFs	$\tau = 10^{-6}$	319	(2.337%)	272	(1.004%)	231	(0.428%)
	$\tau = 10^{-7}$	1496	(10.960%)	1204	(4.444%)	1155	(2.140%)

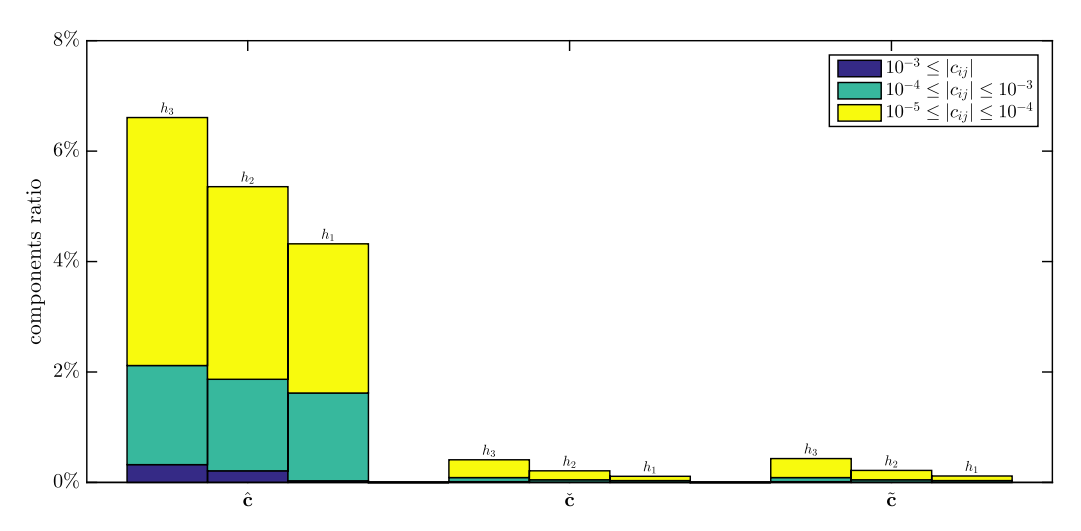


Fig. 5. Components ratios of sparse pattern in  $\hat{\mathbf{c}}$ ,  $\check{\mathbf{c}}$  and  $\tilde{\mathbf{c}}$ .

# 6. Conclusion

A multi-fidelity DCS method is proposed in this paper for the recovery of sparse solution to a stochastic system, in which a data-driven basis is utilized to exploit the sparse patterns. Concerning the two fundamental premises of CS method, namely, the sparsity of expansion coefficients and the requirement on RIP constant of information matrix, the DCS method can enhance the sparsity without changing the RIP constant in compared with typical recovery strategies that use a problem-independent basis. Furthermore, the primary sparse modes remain almost unchanged as the mesh gets refined, which enables us to use the resulting coarse mesh basis for the robust recovery of high-fidelity solution at low cost. Numerical experiments, including some benchmark studies on an elliptic PDE with high-dimensional random input data are carried out to validate our theoretical findings.

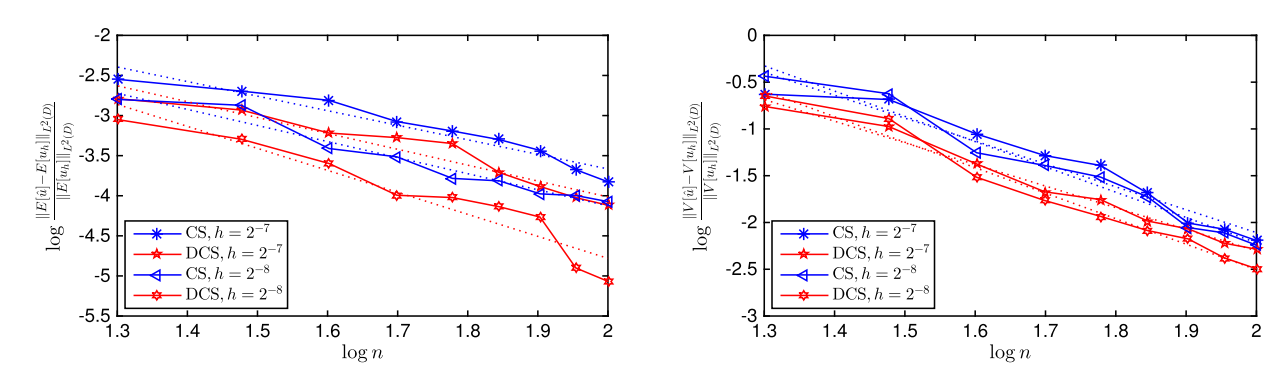


Fig. 6. Error estimates w.r.t. varying sample size (n) and mesh spacing (h).

While our proposed approach has shown much promises, there are various further improvements and extensions that can be investigated. For example, as topics of future research, it is natural to consider possible extensions of the proposed framework to other sparse recovery applications, though new challenges should be addressed. Indeed, when applied to stochastic optimal control problems with PDE state constraints, we expect that the sparse patterns to remain robust w.r.t. the forcing or the boundary condition. This is a subject under ongoing investigation. In addition, one may also consider efficient sampling strategies [23,24], recovery of low-rank solution from both the parametric and physical spaces, and applications to sparse representation of solution to both linear and nonlinear dynamic systems [25,26].

#### Acknowledgements

The work of Qi Sun is partially supported by the NSFC program for Scientific Research Center under program No.: U1530401 and the China Scholarship Council No. 201606340009. The work of Qiang Du is partially supported by US National Science Foundation grant DMS-1719699, US AFOSR MURI Center for Material Failure Prediction Through Peridynamics, and US Army Research Office MURI grant W911NF-15-1-0562.

### Appendix A. Proof of Theorem 3

Note that, by (17), we arrive at the equality (18). Then, by substituting (18) into (14), the covariance function (12) can be written as

$$Cov_{\hat{u}}(x, x') = \sum_{i=2}^{p} \left( \sum_{j=1}^{m} \check{c}_{ij} \phi_{j}(x) \right) \left( \sum_{j'=1}^{m} \check{c}_{ij'} \phi_{j'}(x') \right). \tag{A.1}$$

Next, by substituting (A.1) into (15) and the orthonormality condition  $\langle \phi_k, \phi_{k'} \rangle = \delta_{kk'}$  for  $1 \le k, k' \le m$ , we obtain

$$\lambda_{k}\phi_{k}(x) = \sum_{i=2}^{p} \left( \sum_{j=1}^{m} \check{c}_{ij}\phi_{j}(x) \right) \left( \sum_{j'=1}^{m} \check{c}_{ij'} \int_{D} \phi_{j'}(x')\phi_{k}(x') dx' \right)$$

$$= \sum_{i=2}^{p} \left( \sum_{j=1}^{m} \check{c}_{ij}\check{c}_{ik}\phi_{j}(x) \right) = \sum_{j=1}^{m} \left( \sum_{i=2}^{p} \check{c}_{ij}\check{c}_{ik} \right) \phi_{j}(x),$$
(A.2)

which immediately implies that (19) holds true. Moreover, it can be easily deduced that

$$\mathbb{E}\left[\int_{D} \left(\check{u}(x,\xi) - E_{\check{u}}(x)\right)^{2} dx\right] = \mathbb{E}\left[\sum_{k=1}^{m} \left(\sum_{i=2}^{p} \check{c}_{ik} \psi_{i}(\xi)\right) \left(\sum_{i'=2}^{p} \check{c}_{i'k} \psi_{i'}(\xi)\right)\right]$$
$$= \sum_{k=1}^{m} \left(\sum_{i=2}^{p} |\check{c}_{ik}|^{2}\right) = \sum_{k=1}^{m} \lambda_{k},$$

which completes the proof.

#### Appendix B. Proof of Theorem 4

Step 1. By the orthonormality of basis functions, the projection error (21) can be rewritten as

$$\mathcal{J}(\phi_1, \dots, \phi_m) = \frac{1}{n} \sum_{i=1}^n \mathbb{E} \left[ \| \nu_i \|^2 - \sum_{k=1}^m |\langle \nu_i, \phi_k \rangle|^2 \right]$$
(B.1)

where  $v_i := v(x, \xi_i)$  for simplicity. Then, by the method of Lagrange multiplier, we introduce the multipliers  $\lambda_{m,m'} \in \mathbb{R}$  and define the Lagrangian functional

$$\mathcal{L}(\phi_1,\ldots,\phi_m) = \mathcal{J}(\phi_1,\ldots,\phi_m) + \sum_{k\;k'=1}^m \lambda_{k,k'} \left( \langle \phi_k,\phi_{k'} \rangle - \delta_{kk'} \right).$$

Hence, minimizing  $\mathcal J$  subject to the orthonormality condition  $\langle \phi_k, \phi_{k'} \rangle = \delta_{kk'}$  for  $1 \le k, k' \le m$  is equivalent to finding saddle point of  $\mathcal L$  without constraints, and the first order optimality condition implies

$$\frac{1}{n}\sum_{i=1}^{n}\mathbb{E}\Big[\langle v_i,\phi_k\rangle v_i\Big] = \frac{1}{2}\sum_{k'=1}^{m}(\lambda_{k,k'} + \lambda_{k',k})\phi_{k'} \text{ for } k = 1,\dots,m.$$
(B.2)

Step 2. By defining the operator  $\mathbf{R}$  as

$$\mathbf{R} \phi_k = \frac{1}{n} \sum_{i=1}^n \mathbb{E} \left[ \langle v_i, \phi_k \rangle v_i \right] \text{ for } k = 1, \dots, m,$$

we now proceed by induction to show (B.2) results in the following eigenvalue problem

$$\mathbf{R}\,\phi_{k} = \lambda_{k}\phi_{k}$$
, (B.3)

where  $\lambda_k = \lambda_{k,k}$  for k = 1, ..., m.

For m = 1 we have k, k' = 1, it follows from (B.2) that

$$\mathbf{R} \phi_1 = \frac{1}{2} (\lambda_{1,1} + \lambda_{1,1}) \phi_1 = \lambda_1 \phi_1.$$

Next we suppose that the following equation holds

$$\mathbf{R}\,\phi_k = \lambda_k \phi_k \text{ for } k = 1, \dots, m-1,\tag{B.4}$$

the remaining work is to prove

$$\mathbf{R}\,\phi_m=\lambda_m\phi_m.$$

Due to (B.2), there holds

$$\frac{1}{n}\sum_{i=1}^{n}\mathbb{E}\left[\left\langle v_{i},\phi_{m}\right\rangle v_{i}\right]=\frac{1}{2}\sum_{k'=1}^{m}(\lambda_{m,k'}+\lambda_{k',m})\phi_{k'},\tag{B.5}$$

then by orthogonality condition and inductive hypothesis (B.4), we have for  $\forall 1 \leq k \leq m-1$ ,

$$0 = \lambda_{k} \langle \phi_{m}, \phi_{k} \rangle = \langle \phi_{m}, \mathbf{R} \phi_{k} \rangle = \left\langle \phi_{m}, \frac{1}{n} \sum_{i=1}^{n} \mathbb{E} \left[ \langle v_{i}, \phi_{k} \rangle v_{i} \right] \right\rangle$$

$$= \left\langle \phi_{k}, \frac{1}{n} \sum_{i=1}^{n} \mathbb{E} \left[ \langle v_{i}, \phi_{m} \rangle v_{i} \right] \right\rangle = \left\langle \phi_{k}, \frac{1}{2} \sum_{k'=1}^{m} (\lambda_{m,k'} + \lambda_{k',m}) \phi_{k'} \right\rangle$$

$$= \frac{1}{2} (\lambda_{m,k} + \lambda_{k,m}).$$
(B.6)

Inserting (B.6) into (B.5) we obtain

$$\mathbf{R}\,\phi_m = \frac{1}{2}(\lambda_{m,m} + \lambda_{m,m})\phi_m = \lambda_m\phi_m,$$

which complete the proof of induction.

Step 3. In what follows, we show the eigenvalue problem (B.3) is nothing but the integral equation (15) and therefore the representation derived from Algorithm 2 does best, among all such expansions involving spatial orthonormal basis of dimension m, at capturing the energy of sample observations.

By (17) and (18), it can be deduced that

$$\mathbf{R}\,\phi_{k} = \frac{1}{n}\sum_{j=1}^{n}\mathbb{E}\Big[\langle \mathbf{v}_{i},\phi_{k}\rangle\,\mathbf{v}_{i}\Big] = \frac{1}{n}\sum_{i=1}^{n}\left[\sum_{i'=2}^{p}\left\langle\sum_{j=1}^{m}\hat{c}_{i'j}\phi_{j},\phi_{k}\right\rangle\left(\sum_{j=1}^{m}\hat{c}_{i'j}\phi_{j}\right)\right]$$

$$= \frac{1}{n}\sum_{i=1}^{n}\left[\sum_{i'=2}^{p}\left\langle\sum_{j=1}^{m}\check{c}_{i'j}\phi_{j},\phi_{k}\right\rangle\left(\sum_{j=1}^{m}\check{c}_{i'j}\phi_{j}\right)\right]$$

$$= \frac{1}{n}\sum_{i=1}^{n}\left(\sum_{i'=2}^{p}\sum_{j=1}^{m}\check{c}_{i'j}\check{c}_{i'k}\phi_{j}\right)$$

$$= \sum_{i=2}^{p}\left(\sum_{j=1}^{m}\check{c}_{ij}\check{c}_{ik}\right)\phi_{j} = \int_{D}\operatorname{Cov}_{\hat{u}}(x,x')\phi_{k}(x')\,dx',$$
(B.7)

where the last equality holds by (A.2). Hence, the basis functions  $\{\phi_j(x)\}_{j=1}^m$  derived from the integral equation (B.3) minimize the projective error (21).

#### References

- [1] M.D. Gunzburger, C.G. Webster, G. Zhang, Stochastic finite element methods for partial differential equations with random input data, Acta Numer. 23 (2014) 521–650.
- [2] D. Xiu, Fast numerical methods for stochastic computations: a review, Commun. Comput. Phys. 5 (2009) 242–272.
- [3] A. Doostan, H. Owhadi, A non-adapted sparse approximation of pdes with stochastic inputs, J. Comput. Phys. 230 (2011) 3015-3034.
- [4] X. Yang, H. Lei, N.A. Baker, G. Lin, Enhancing sparsity of Hermite polynomial expansions by iterative rotations, J. Comput. Phys. 307 (2016) 94-109.
- [5] X. Yang, X. Wan, L. Lin, A general framework of enhancing sparsity of generalized polynomial chaos expansions, arXiv:1707.02688, 2017.
- [6] J. Burkardt, Q. Du, M. Gunzburger, H.-C. Lee, Reduced order modeling of complex systems, in: D.F. Griffiths, G.A. Watson (Eds.), Proceeding of the 20th Biennial Conference on Numerical Analysis, University of Dundee, 2003, pp. 29–38.
- [7] Q. Du, M.D. Gunzburger, Centroidal Voronoi tessellation based proper orthogonal decomposition analysis, in: Control and Estimation of Distributed Parameter Systems, Springer, 2003, pp. 137–150.
- [8] M. Gunzburger, J. Ming, Optimal control of stochastic flow over a backward-facing step using reduced-order modeling, SIAM J. Sci. Comput. 33 (2011) 2641–2663.
- [9] C. Schwab, C.J. Gittelson, Sparse tensor discretizations of high-dimensional parametric and stochastic pdes, Acta Numer. 20 (2011) 291-467.
- [10] T. Tang, T. Zhou, Recent developments in high order numerical methods for uncertainty quantification, Sci. Sin., Math. 45 (2015) 891–928.
- [11] A.M. Bruckstein, D.L. Donoho, M. Elad, From sparse solutions of systems of equations to sparse modeling of signals and images, SIAM Rev. 51 (2009) 34–81.
- [12] Y. Gwon, H. Kung, D. Vlah, Compressive sensing with optimal sparsifying basis and applications in spectrum sensing, in: Global Communications Conference, GLOBECOM, IEEE, 2012, pp. 5386–5391.
- [13] E.J. Candès, J. Romberg, T. Tao, Robust uncertainty principles: Exact signal reconstruction from highly incomplete frequency information, IEEE Trans. Inf. Theory 52 (2006) 489–509.
- [14] J.D. Jakeman, M.S. Eldred, K. Sargsyan, Enhancing  $\ell_1$ -minimization estimates of polynomial chaos expansions using basis selection, J. Comput. Phys. 289 (2015) 18–34
- [15] B. Peherstorfer, K. Willcox, M. Gunzburger, Survey of multifidelity methods in uncertainty propagation, inference, and optimization, arXiv:1806.10761,
- [16] M. Cheng, T.Y. Hou, M. Yan, Z. Zhang, A data-driven stochastic method for elliptic pdes with random coefficients, SIAM/ASA J. Uncertain. Quantificat. 1
- [17] D. Xiu, G.E. Karniadakis, The Wiener-Askey polynomial chaos for stochastic differential equations, SIAM J. Sci. Comput. 24 (2002) 619-644.
- [18] M.K. Deb, I.M. Babuška, J.T. Oden, Solution of stochastic partial differential equations using Galerkin finite element techniques, Comput. Methods Appl. Mech. Eng. 190 (2001) 6359–6372.
- [19] E.J. Candes, The restricted isometry property and its implications for compressed sensing, C. R. Math. 346 (2008) 589-592.
- [20] S. Jokar, Sparse recovery and Kronecker products, in: 44th Annual Conference on Information Sciences and Systems, CISS, IEEE, 2010, pp. 1-4.
- [21] P. Frauenfelder, C. Schwab, R.A. Todor, Finite elements for elliptic problems with stochastic coefficients, Comput. Methods Appl. Mech. Eng. 194 (2005) 205–228.
- [22] R.C. Smith, Uncertainty Quantification: Theory, Implementation, and Applications, SIAM, 2013.
- [23] J. Hampton, A. Doostan, Coherence motivated sampling and convergence analysis of least squares polynomial chaos regression, Comput. Methods Appl. Mech. Eng. 290 (2015) 73–97.
- [24] J.D. Jakeman, A. Narayan, T. Zhou, A generalized sampling and preconditioning scheme for sparse approximation of polynomial chaos expansions, SIAM J. Sci. Comput. 39 (2017) A1114–A1144.
- [25] J.N. Kutz, S.L. Brunton, B.W. Brunton, J.L. Proctor, Dynamic Mode Decomposition: Data-Driven Modeling of Complex Systems, SIAM, 2016.
- [26] T. Li, Q. Du, Abstract principal component analysis, Sci. China Math. 56 (2013) 2783–2798.